

Surface-Pt-rich AgPtAu trimetallic nanotrough array for boosting alcohol electrooxidation

Jing-Jing Li,^a Wen-Chao Geng,^b Ling Jiang^a and Yong-Jun Li*^a

^a State Key Lab of Chemo/Biosensing and Chemometrics, College of Chemistry and Chemical Engineering, Hunan University, Changsha 410082, China. E-mail: liyje@hnu.edu.cn; Tel: +86-731-88821603

^b School of Chemical and Printing-Dyeing Engineering, Henan University of Engineering, Zhengzhou 450000, China

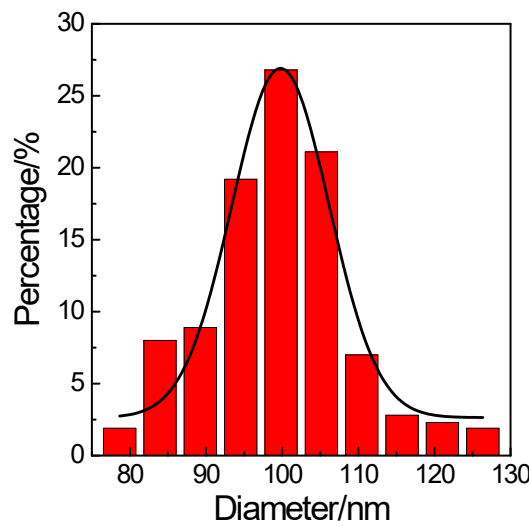


Fig. S1 Diameter distribution of Ag nanowires.

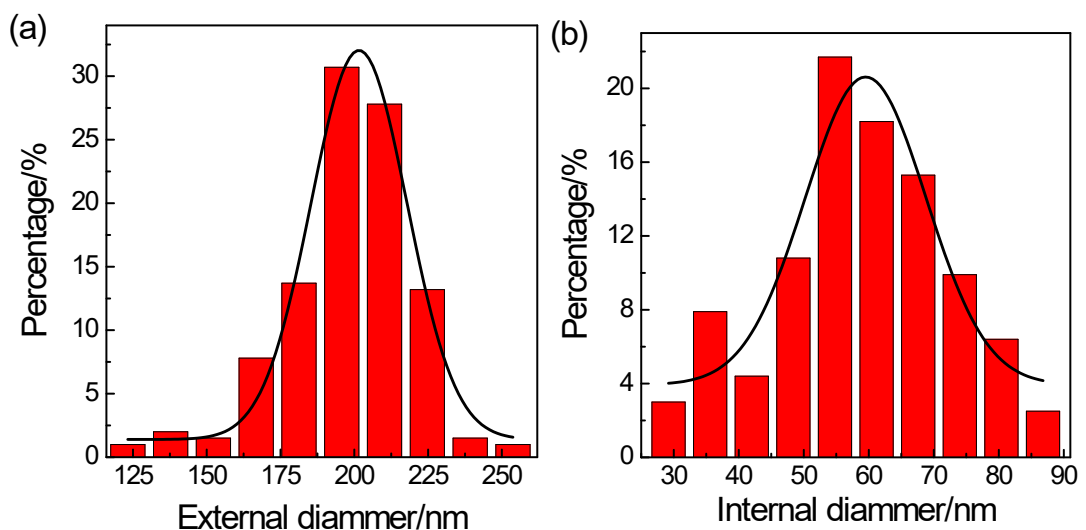


Fig. S2 External (a) and internal (b) diameter distribution of $\text{Ag}_{11}\text{Pt}_5\text{Au}_{84}$.

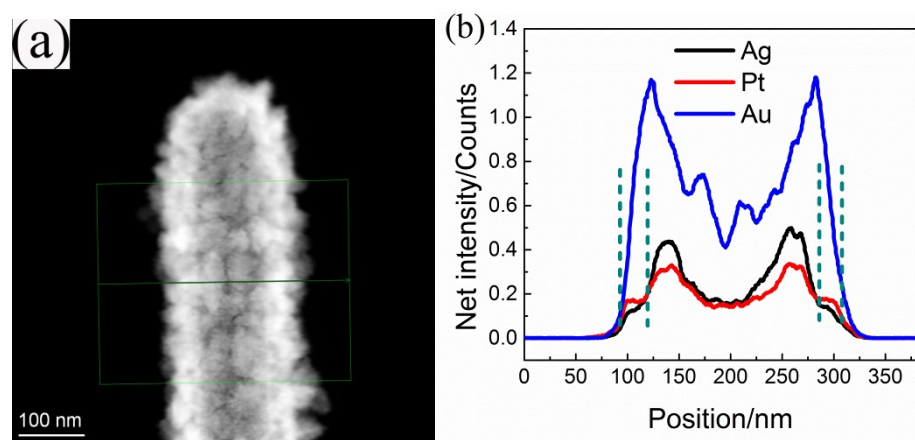


Fig. S3 HAADF image (a) and linear scan element-distribution profile (b) of $\text{Ag}_{11}\text{Pt}_5\text{Au}_{84}$ nanostructure.

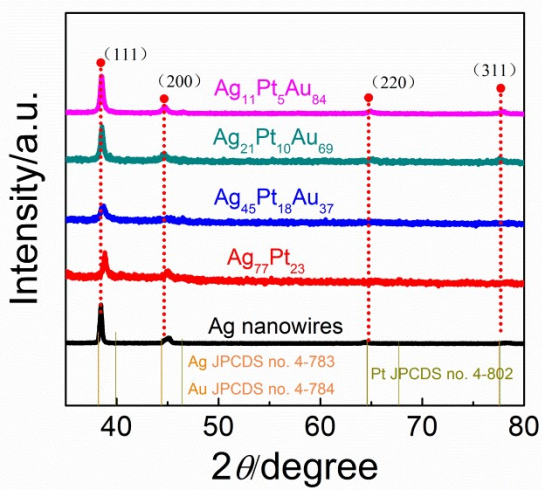


Fig. S4 XRD patterns of Ag nanowires, $\text{Ag}_{77}\text{Pt}_{23}$, $\text{Ag}_{45}\text{Pt}_{18}\text{Au}_{37}$, $\text{Ag}_{21}\text{Pt}_{10}\text{Au}_{69}$ and $\text{Ag}_{11}\text{Pt}_5\text{Au}_{84}$ nanostructure. For comparison, standard diffraction peak centers of Ag (JCPDS no. 4-783), Au (JCPDS no. 4-784), and Pt (JCPDS no. 4-802) were marked.

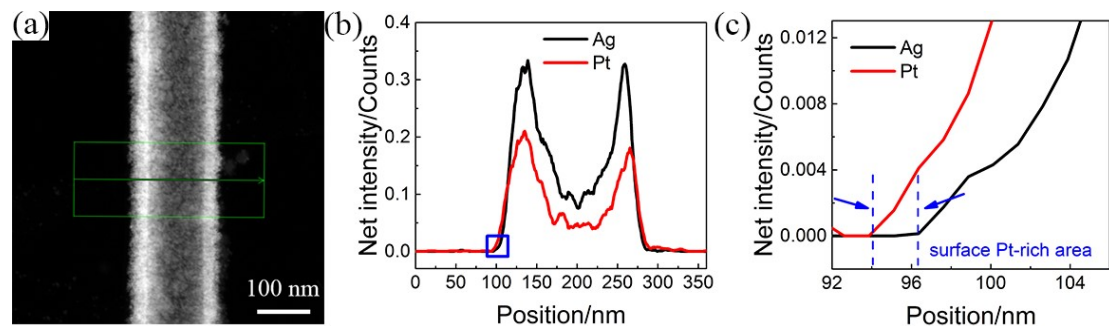


Fig. S5 HAADF image (a) and linear scan element-distribution profile (b,c) of $\text{Ag}_{77}\text{Pt}_{23}$ nanostructure. Graph c is the enlargement of the part of graph b, as marked in blue box in graph b.

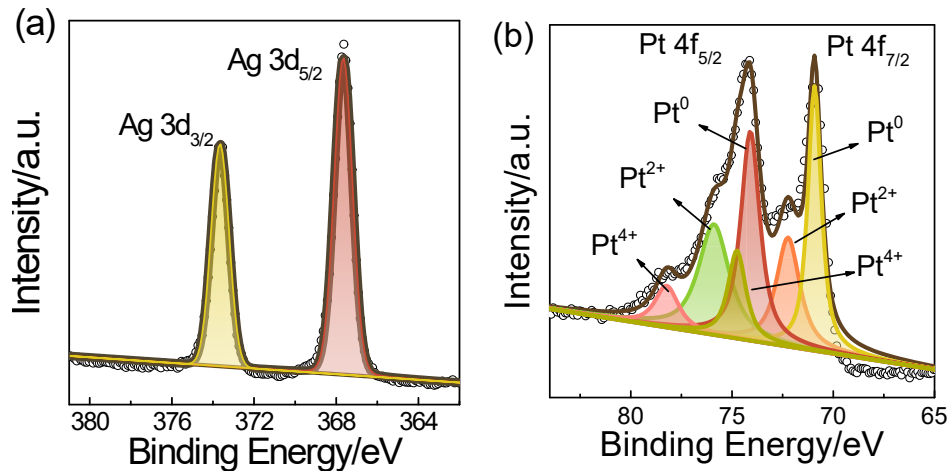


Fig. S6 XPS spectra of Ag 3d (a) and Pt 4f (b) of Ag₇₇Pt₂₃. The black circle and the brown solid curves are the original data and the fitted curves, respectively, and other colorful curves are the deconvoluted ones.

XPS characterization shows that the energy band of Ag of Ag₇₇Pt₂₃ is perfectly symmetrical, consistent with the standard patterns of Ag⁰ 3d and Au⁰ 4f,¹ indicating that Ag species is in the metallic state. Nevertheless, compared with Ag nanowire (Ag 3d_{5/2}, 367.4 eV; 3d_{3/2}, 373.4 eV),² Ag 3d_{5/2} and 3d_{3/2} of Ag₇₇Pt₂₃ are located at higher energy (Fig. S6a); Pt⁰ 4f_{7/2} and 4f_{5/2} binding energy bands are centered at 70.88 and 74.25 eV, respectively (Fig. S6b), ~0.32 eV shift towards the lower energy direction when compared with pure Pt (4f_{7/2}, 71.20 eV; 4f_{5/2}, 74.53 eV). These results indicate that, due to the small electronegativity of Ag (1.93),³ more electrons accumulate around Pt,⁴ which may modify the electronic structure of Ag₇₇Pt₂₃, helpful for improving the tolerance of Pt towards CO-like species.^{5, 6} Additionally, Pt 4f binding energy shows shoulder bands owing to the existence of Pt²⁺ and Pt⁴⁺, which can be attributed to platinum oxide.⁷

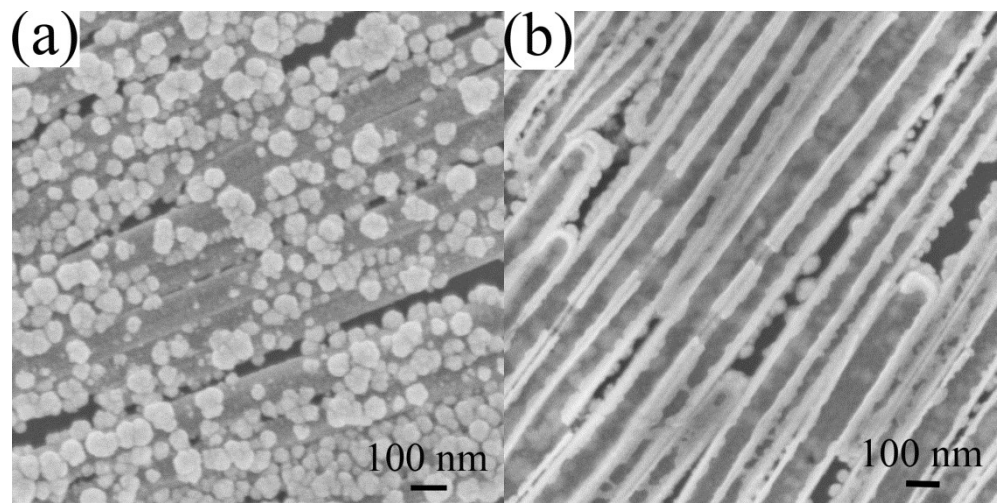


Fig. S7 SEM image of AgPtAu nanostructure with high-purified Ag nanowires as the starting material: the bottom side (a) and top side (b).

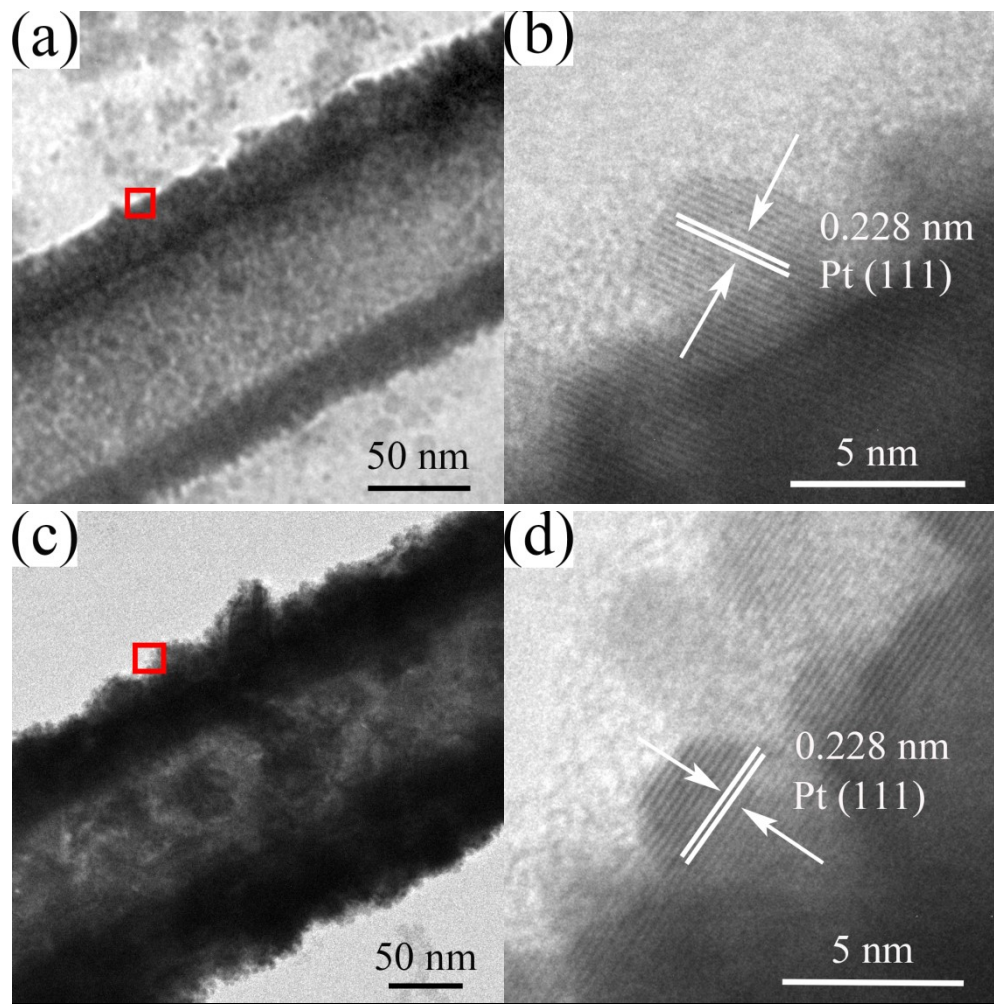


Fig. S8 TEM (a,c) and HRTEM (b,d) images of $\text{Ag}_{45}\text{Pt}_{18}\text{Au}_{37}$ (a,b) and $\text{Ag}_{21}\text{Pt}_{10}\text{Au}_{69}$ (c,d).

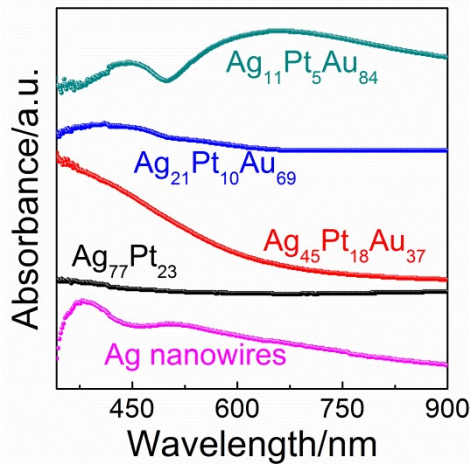


Fig. S9 UV-vis spectra of Ag nanowire, $\text{Ag}_{77}\text{Pt}_{23}$, $\text{Ag}_{45}\text{Pt}_{18}\text{Au}_{37}$, $\text{Ag}_{21}\text{Pt}_{10}\text{Au}_{69}$, and $\text{Ag}_{11}\text{Pt}_5\text{Au}_{84}$ redispersed in ethanol.

Ag nanowire shows two absorption peaks centered at ~378.6 and 516.0 nm, corresponding to its transversal and longitudinal plasma resonances,⁸ respectively. By contrast, $\text{Ag}_{77}\text{Pt}_{23}$ almost does not show any absorption owing to the damping effect of Pt.^{9, 10} Although the introduction of Au into $\text{Ag}_{77}\text{Pt}_{23}$ reduces the content of Ag, it simultaneously decreases the content of Pt, lowering the damping effect of Pt. Composition-varied AgPtAu nanostructures show different absorption features. $\text{Ag}_{45}\text{Pt}_{18}\text{Au}_{37}$ shows a broad absorption between ~360 and 650 nm, the part of which lower than 450 nm may be attributed to Ag transversal plasma resonance and the part of which larger than 450 nm may be attributed to Au plasma resonance. With the increase of Au content, a well-defined absorption pattern is obtained for $\text{Ag}_{11}\text{Pt}_5\text{Au}_{84}$.

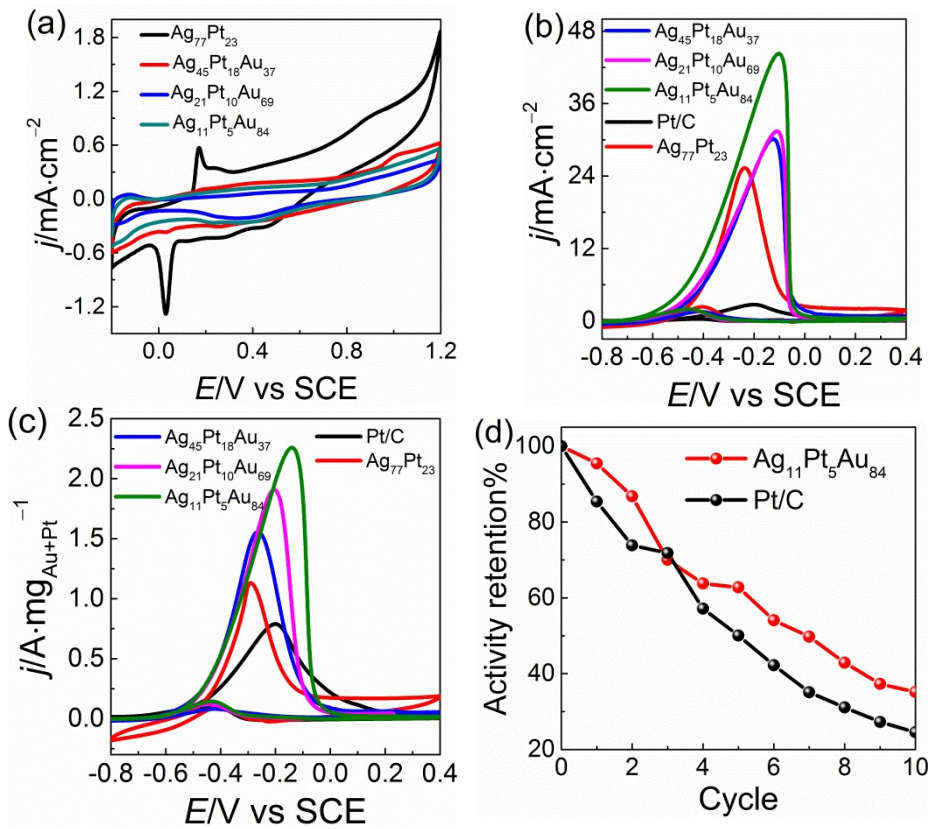


Fig. S10 ECSA- (a) cyclic voltammograms for Pt/C, $\text{Ag}_{77}\text{Pt}_{23}$, $\text{Ag}_{45}\text{Pt}_{18}\text{Au}_{37}$, $\text{Ag}_{21}\text{Pt}_{10}\text{Au}_{69}$, and $\text{Ag}_{11}\text{Pt}_5\text{Au}_{84}$ in N_2 -saturated $0.5 \text{ mol L}^{-1} \text{H}_2\text{SO}_4$, 50 mV s^{-1} ; ECSA- (b) and mass-normalized (c) cyclic voltammograms for Pt/C, $\text{Ag}_{77}\text{Pt}_{23}$, $\text{Ag}_{45}\text{Pt}_{18}\text{Au}_{37}$, $\text{Ag}_{21}\text{Pt}_{10}\text{Au}_{69}$, and $\text{Ag}_{11}\text{Pt}_5\text{Au}_{84}$ in N_2 -saturated $1.0 \text{ mol L}^{-1} \text{KOH} + 1.0 \text{ mol L}^{-1} \text{CH}_3\text{OH}$, 50 mV s^{-1} ; (d) activity retention of Pt/C and $\text{Ag}_{11}\text{Pt}_5\text{Au}_{84}$ based on the cyclic voltammetric data of each operation cycle in N_2 -saturated $1.0 \text{ mol L}^{-1} \text{KOH} + 1.0 \text{ mol L}^{-1} \text{CH}_3\text{OH}$ (900 s amperometric measurement and subsequently a cyclic voltammetric sweeping from -0.40 to 0.80 V as an operation cycle).

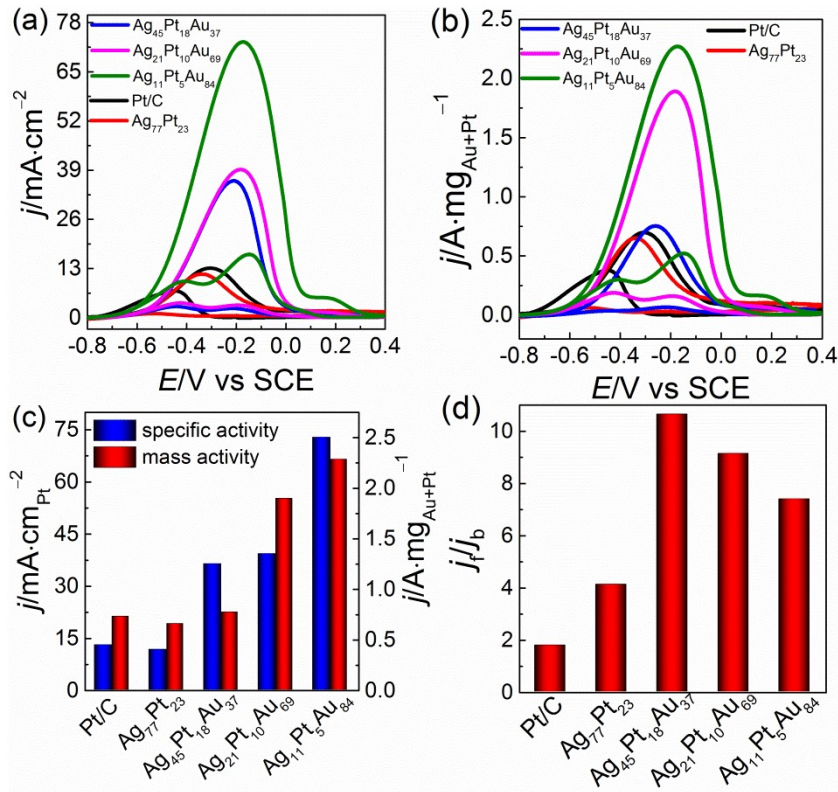


Fig. S11 ECSA- (a) and mass-normalized (b) cyclic voltammograms for Pt/C, $Ag_{77}Pt_{23}$, $Ag_{45}Pt_{18}Au_{37}$, $Ag_{21}Pt_{10}Au_{69}$, and $Ag_{11}Pt_5Au_{84}$ in N_2 -saturated 1.0 mol L^{-1} KOH + 1.0 mol L^{-1} CH_3CH_2OH , 50 mV s^{-1} ; (c) summary of specific activity of Pt/C, $Ag_{77}Pt_{23}$, $Ag_{45}Pt_{18}Au_{37}$, $Ag_{21}Pt_{10}Au_{69}$, and $Ag_{11}Pt_5Au_{84}$ towards methanol oxidation; (d) comparison of j_f/j_b of mass-normalized cyclic voltammograms.

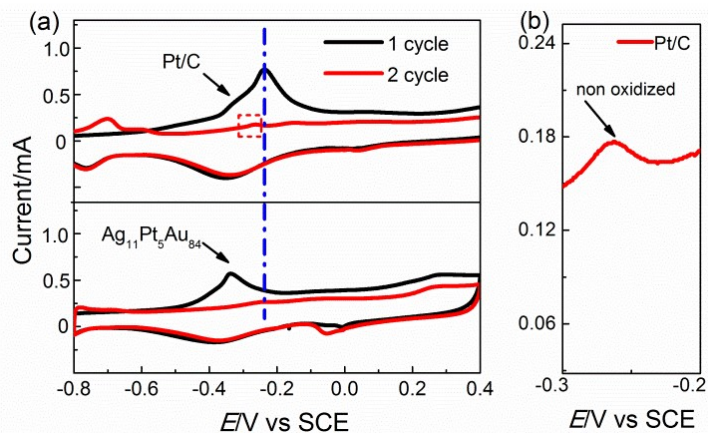


Fig. S12 Cyclic voltammograms of CO-saturated adsorbed $\text{Ag}_{11}\text{Pt}_5\text{Au}_{84}$ nanotrough array and CO-saturated adsorbed Pt/C in 1.0 mol·L⁻¹ KOH ($v = 50 \text{ mV}\cdot\text{s}^{-1}$).

Excellent anti-poisoning ability of $\text{Ag}_{11}\text{Pt}_5\text{Au}_{84}$ is further confirmed by CO stripping experiments (Fig. S12). CO oxidation peak is centered at -0.33 V at $\text{Ag}_{11}\text{Pt}_5\text{Au}_{84}$, $\sim 100 \text{ mV}$ negative than that of commercial Pt/C (-0.23 V) (Fig. S12a), suggesting that CO desorption is much easier from $\text{Ag}_{11}\text{Pt}_5\text{Au}_{84}$. In the second cycle, CO characteristic peak completely disappears at $\text{Ag}_{11}\text{Pt}_5\text{Au}_{84}$ whereas it does not at Pt/C, indicating that $\text{Ag}_{11}\text{Pt}_5\text{Au}_{84}$ is capable of oxidizing CO completely (Fig. S12b).

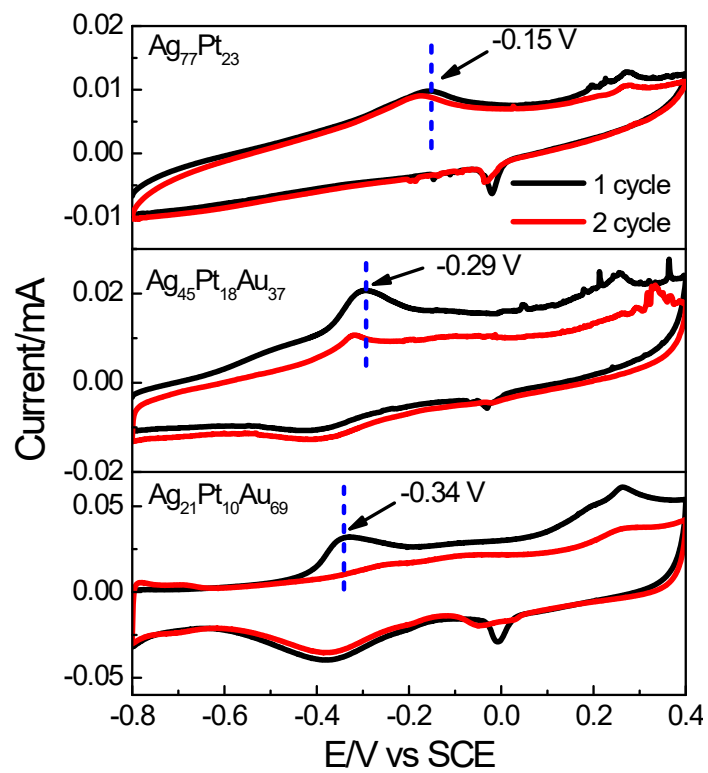


Fig. S13 Cyclic voltammograms of CO-saturated adsorbed $\text{Ag}_{77}\text{Pt}_{23}$, $\text{Ag}_{45}\text{Pt}_{18}\text{Au}_{37}$, $\text{Ag}_{21}\text{Pt}_{10}\text{Au}_{69}$ nanotrough array in $1.0 \text{ mol}\cdot\text{L}^{-1}$ KOH ($v = 50 \text{ mV}\cdot\text{s}^{-1}$).

Table S1. The atomic ratios of AgPt and AgPtAu samples determined by ICP-OES technique.

Catalyst	Volume (μL)		Atomic ratio Ag:Pt:Au
	H_2PtCl_6	HAuCl_4	
$\text{Ag}_{77}\text{Pt}_{23}$	35	0	77:23:0
$\text{Ag}_{45}\text{Pt}_{18}\text{Au}_{37}$	35	20	45:18:37
$\text{Ag}_{21}\text{Pt}_{10}\text{Au}_{69}$	35	50	21:10:69
$\text{Ag}_{11}\text{Pt}_5\text{Au}_{84}$	35	100	11:5:84

Table S2. Catalyst loading of different elements (which were determined by ICP-OES) on the surface of the glassy carbon electrode and its electrochemical active surface area (ECSA) toward alcohol in the alkaline solution.

Catalyst	catalyst loading of Au/ μ g	catalyst loading of Pt/ μ g	ECSA/ m^2 g $_{Pt}^{-1}$
Pt/C	/	5	29
Ag ₇₇ Pt ₂₃	/	0.254	5.4
Ag ₄₅ Pt ₁₈ Au ₃₇	0.629	0.293	35.6
Ag ₂₁ Pt ₁₀ Au ₆₉	2.696	0.373	39.7
Ag ₁₁ Pt ₅ Au ₈₄	3.853	0.217	55

Table S3. Summary of the electrocatalytic oxidation performance of AgPtAu nanostructure in our case and other previously reported catalysts towards methanol in the alkaline solution.

Catalyst	ECSA-normalized activity (mA·cm ⁻²)	Mass-normalized activity	Reference
Au/Ag/Pt alloy nanoparticles	0.13	1.699 A mg _{Pt} ⁻¹	11
Au/Ag/Pt hetero-nanostructure	1.40	1 A mg _{Pt} ⁻¹	12
3D Pt/C composite	/	0.426 A mg _{Pt} ⁻¹	13
Au@AgPt yolk-shell nanoparticles	0.7	0.9 A mg _{Pt} ⁻¹	14
AgAu@Pt nanoframes	/	0.483 A mg _{Pt} ⁻¹	15
Pt-nanoporous gold Au leaf	1.65	1.06 A mg _{Pt} ⁻¹	16
Pt/C	2.8	0.796 A mg _{Pt} ⁻¹	This work
Ag ₇₇ Pt ₂₃	25.32	1.137 A mg _{Au+Pt} ⁻¹	This work
Ag ₄₅ Pt ₁₈ Au ₃₇	30.26	1.565 A mg _{Au+Pt} ⁻¹	This work
Ag ₂₁ Pt ₁₀ Au ₆₉	31.59	1.919 A mg _{Au+Pt} ⁻¹	This work
Ag ₁₁ Pt ₅ Au ₈₄	44.00	2.26 A mg _{Au+Pt} ⁻¹	This work

Table S4. Summary of the electrocatalytic oxidation performance of AgPtAu nanostructure in our case and other previously reported catalysts towards ethanol in the alkaline solution.

Catalyst	ECSA-normalized activity (mA·cm ⁻²)	Mass-normalized activity	Reference
22% YO _x /MoO _x -Pt NWs	2.59	1.63 A mg _{Pt} ⁻¹	¹⁷
Au/Pt nanodendrites	30	/	¹⁸
Pt ₃ Rh ₁ Ni ₂ nanoassemblies	8	1.4 A mg _{metal} ⁻¹	¹⁹
Pt/NiCe ₄	/	0.087 A mg _{Pt} ⁻¹	²⁰
Pt/C	2.8	0.770 A mg _{Pt} ⁻¹	This work
Ag ₇₇ Pt ₂₃	11.50	0.663 A mg _{Au+Pt} ⁻¹	This work
Ag ₄₅ Pt ₁₈ Au ₃₇	36.36	0.764 A mg _{Au+Pt} ⁻¹	This work
Ag ₂₁ Pt ₁₀ Au ₆₉	39.67	1.9 A mg _{Au+Pt} ⁻¹	This work
Ag ₁₁ Pt ₅ Au ₈₄	73.00	2.29 A mg _{Au+Pt} ⁻¹	This work

References

1. J. Moulder, J. Chastain and R. King, *Chem. Phys. Lett.*, 1995, **220**, 7-10.
2. H. Mao, J. Feng, X. Ma, C. Wu and X. Zhao, *J Nanopart Res.*, 2012, **14**, 1-15.
3. X. Fu, C. Wan, A. Zhang, Z. Zhao, H. Huyan, X. Pan, S. Du, X. Duan and Y. Huang, *Nano Res.*, 2020, **13**, 1472-1478.
4. J. Yang and J. Y. Ying, *Angew. Chem. Int. Ed.*, 2011, **50**, 4637-4643.
5. J. H. Kim, S. M. Choi, S. H. Nam, M. H. Seo, S. H. Choi and W. B. Kim, *Appl. Catal. B*, 2008, **82**, 89-102.
6. H. H. Li, S. Zhao, M. Gong, C. H. Cui, D. He, H. W. Liang, L. Wu and S. H. Yu, *Angew. Chem. Int. Ed.*, 2013, **52**, 7472-7476.
7. J. Sun, T. Li, X. Li, J. Pan, X. Hao and T. Zhu, *J. Alloys Compd.*, 2020, **831**, 154871.
8. P. Chandrasekhar, H. Elbohy, B. Vaggensmith, A. Dubey, K. M. Reza, V. K. Komarala and Q. Qiao, *Materials Today Energy*, 2017, **5**, 237-242.
9. J. Heo, D. S. Kim, Z. H. Kim, Y. W. Lee, D. Kim, M. Kim, K. Kwon, H. J. Park, S. Y. Wan and W. H. Sang, *Chem. Commun.*, 2008, **46**, 6120-6122.
10. Y. W. Lee, M. Kim, Z. H. Kim and S. W. Han, *J. Am. Chem. Soc.*, 2009, **131**, 17036-17037.
11. R. Sarkar, A. A. Farghaly and I. U. Arachchige, *Chem. Mater.*, 2022, **34**, 5874-5887.
12. X. Xie, G. Gao, S. Kang, T. Shibayama, Y. Lei, D. Gao and L. Cai, *Adv. Mater.*, 2015, **27**, 5573-5577.
13. Ding. T, Zhang. L, Li. H, Sun. Y and Yang. Q, *ACS Omega*, 2018, **3**, 17668-17675.
14. N. Sui, R. Yue, Y. Wang, Q. Bai, R. An, H. Xiao, L. Wang, M. Liu and W. W. Yu, *J. Alloys Compd.*, 2019, **790**, 792-798.
15. X. Yan, S. Yu, Y. Tang, D. Sun, L. Xu and C. Xue, *Nanoscale*, 2018, **10**, 2231-2235.
16. X. Ge, R. Wang, P. Liu and Y. Ding, *Chem. Mater.*, 2007, **19**, 5827-5829.
17. M. Li, Z. Zhao, W. Zhang, M. Luo, L. Tao, Y. Sun, Z. Xia, Y. Chao, K. Yin and Q. Zhang, *Adv. Mater.*, 2021, **33**, 2103762.
18. W. Chen, S. Luo, M. Sun, X. Wu, Y. Zhou, Y. Liao, M. Tang, X. Fan, B. Huang and Z. Quan, *Adv. Mater.*, 2022, **34**, 2206276.
19. H. Liu, J. Li, L. Wang, Y. Tang, B. Y. Xia and Y. Chen, *Nano Res.*, 2017, **10**, 3324-3332.
20. Z. Xu, L. Rao, H. Song, Z. Yan, L. Zhang and S. Yang, *Chinese. J. Catal.*, 2017, **38**, 305-312.